International Journal of Astrobiology 14 (3): 517–526 (2015) doi:10.1017/S1473550415000026

The structure and chemical layering of Proterozoic stromatolites in the Mojave Desert

Susanne Douglas[1,2], Meredith E. Perry[3,4], William J. Abbey[5], Zuki Tanaka[4,6], Bin Chen[4,6] and Christopher P. McKay[4]

[1]*Planetary Science Institute, Tucson, AZ 85719, USA*
[2]*East Los Angeles College, Monterey Park, CA 91754, USA*
[3]*Department of Earth and Environmental Science, University of Pennsylvania, Philadelphia PA 19104, USA*
[4]*NASA Ames Research Center, Moffett Field, CA 940356, USA*
e-mail: chris.mckay@nasa.gov
[5]*JPL, Pasadena, CA 91109, USA*
[6]*Department of Electrical Engineering, UC Santa Cruz, Santa Cruz, CA 95060, USA*

Abstract: The Proterozoic carbonate stromatolites of the Pahrump Group from the Crystal Spring formation exhibit interesting layering patterns. In continuous vertical formations, there are sections of chevron-shaped stromatolites alternating with sections of simple horizontal layering. This apparent cycle of stromatolite formation and lack of formation repeats several times over a vertical distance of at least 30 m at the locality investigated. Small representative samples from each layer were taken and analysed using X-ray diffraction (XRD), X-ray fluorescence (XRF), environmental scanning electron microscopy – energy dispersive X-ray spectrometry, and were optically analysed in thin section. Optical and spectroscopic analyses of stromatolite and of non-stromatolite samples were undertaken with the objective of determining the differences between them. Elemental analysis of samples from within each of the four stromatolite layers and the four intervening layers shows that the two types of layers are chemically and mineralogically distinct. In the layers that contain stromatolites the Ca/Si ratio is high; in layers without stromatolites the Ca/Si ratio is low. In the high Si layers, both K and Al are positively correlated with the presence and levels of Si. This, together with XRD analysis, suggested a high K-feldspar (microcline) content in the non-stromatolitic layers. This variation between these two types of rocks could be due to changes in biological growth rates in an otherwise uniform environment or variations in detrital influx and the resultant impact on biology. The current analysis does not allow us to choose between these two alternatives. A Mars rover would have adequate resolution to image these structures and instrumentation capable of conducting a similar elemental analysis.

Received 16 October 2014, accepted 20 December 2014, first published online 9 March 2015

Key words: stromatolite, Mars, elemental analysis

Introduction

Biogenic stromatolites are organo-sedimentary structures formed by the metabolic activity of photosynthetic microorganisms, often cyanobacteria. Microorganisms release biomolecules that combine with surrounding sediment to form alternating layers, whereas the phototactic motion of the microorganisms mould the layers into characteristic dome and chevron shapes (e.g. Grotzinger & Knoll 1999). Of particular interest to those studying ancient life, stromatolites are the oldest known evidence of life on the Earth. The oldest probable stromatolites are in the c. 3.48 Gyr old Dresser Formation (Walter *et al.* 1980; Hickman 2011; Wacey 2012). The more convincing stromatolites in the Strelley Pool Formation are now dated at 3.43–3.35 Gyr ago (Lowe 1980; Hofmann *et al.* 1999; Allwood *et al.* 2006; Hickman 2011). Because they are large structures produced by microbial life stromatolites are also potential targets for the search for life on Mars, (McKay 1986; McKay & Stoker 1989).

Studies of the physical form, mineralogical composition and organic inclusions of stromatolites can reveal information about the environments under which they formed. Tice & Lowe (2004) inferred that deposition of some of the oldest stromatolites known (the 3.4 Ga Buck Reef Chert in South Africa) occurred in open shallow to deep marine environments with a stratified early ocean. In this scenario, carbonaceous matter was formed by photosynthetic mats within the euphotic zone and distributed as detrital matter by waves and currents to surrounding environments. Allwood *et al.* (2006) concluded from their study of stromatolites from the Strelley Pool Chert that the local formation environment was a broad peritidal platform that resulted in reef-like build-up of biogenic structures

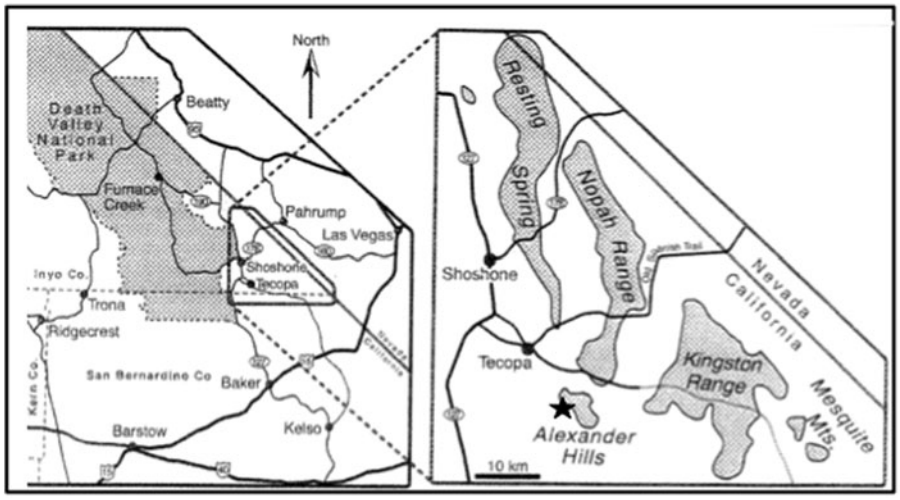

Fig. 1. Map showing site location just east of Death Valley National Park approximately 30 km south-southeast of Shoshone, California (N35.78806°, W116.12701° elevation 711 m).

in shallow water as surfaces became submerged. Buick (2008) reviewed information on stromatolite form and occurrence to better understand the development of oxygenic photosynthesis. Recently, Corkeron *et al.* (2012) examined geochemical variation between stromatolitic and non-stromatolitic deposits in the Neoproterozoic Loves Creek Member, Bitter Springs Formation of the Amadeus Basin, a unit slightly younger that the one described here. They compared the geochemistry of stromatolitic columns with the column interspaces, rather than interbedded sediment, with a focus on Rare Earth Elements. That study indicated significant differences between the chemistry of abiogenically and biogenically formed structures. These studies illustrate the extent of paleoenvironmental data that can be derived from stromatolites and further motivate the search for stromatolites on Mars.

The stromatolites found in the PreCambrian Crystal Spring Formation (Pahrump Group) near Death Valley, California (Fig. 1), provide an opportunity to study alternating layers of sediments with and without stromatolites present. The morphology and growth pattern of these stromatolites has previously been well-documented (Howell 1971). Awramik *et al.* (2000) also reviewed the available information on the age of the Crystal Springs carbonate formation and concluded that they are 1.5 ± 0.2 Gyr old. Our study location is a single carbonate section forming a nearly vertical face located in the Alexander Hills. These stromatolites are unusual also for the fact that their mineral matrix is calcite, rather than the more commonly encountered dolomite or chert. Our interest in this site stems from this aspect and also from a wish to gain an understanding of the environmental conditions that appear to have varied at this site in such a way as to promote repeated cycles of stromatolite formation interspersed with a lack of stromatolites. In this paper, we report on the mineralogical and elemental trends found within the stromatolite and non-stromatolite bearing layers, similar to the approach of Corkeron *et al.* (2012).

Methods

Field approach

The section of interest contains repeated cycles of progressive stromatolite growth, wavy laminae grading upwards into chevron-shaped heads, separated by laterally continuous zones of a much harder, dark material (see Figs 2 and 3). Samples were taken by hammer and chisel from each section as labelled in Fig. 2, one from each of the four stromatolite layers and one from each of the accompanying non-stromatolitic layers – eight samples in total.

Petrography & Raman Spectroscopy

Petrography was performed on a Leica DM 4500 polarizing light microscope with standard 30 μm thin sections (no cover slips) using both transmitted and reflected light. Confirmation of mineral identifications was done on a Horiba Jobin Yvon LabRam HR confocal Raman microscope/spectrometer. Point spectra were obtained on select mineral grains using an excitation wavelength of 532 nm (spot size ~5 μm) and a 50 × (0.75 N.A.) long working distance objective. Phase identification was confirmed by comparing acquired Raman spectra with reference spectra from the RRUFF database, hosted by the University of Arizona (Downs 2006).

X-ray diffraction (XRD)

Bulk mineralogy of select samples was determined by obtaining powder XRD patterns using a Bruker AXS model D8 Discover X-ray diffractometer equipped with a graphite monochromator and a General Area Detector Diffraction System (GADDS). Radiation applied was CuKα (λ = 1.5404 Å) operated at 40 kV and 20 mA. Phase identification was confirmed by comparing the 20–54° 2 thetas; range with standard powder diffraction files from the International Centre for Diffraction

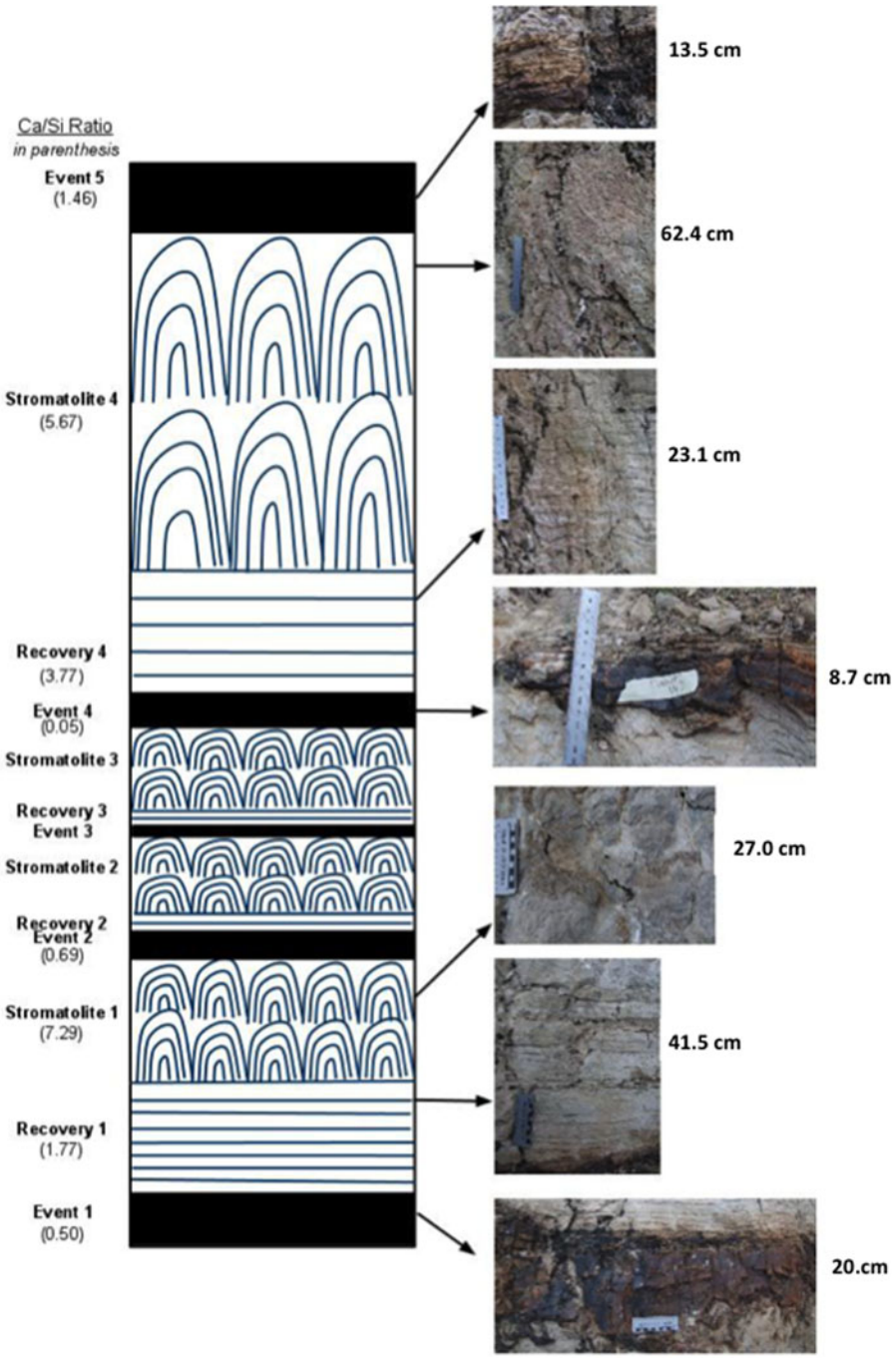

Fig. 2. Diagram of the section under study showing the occurrence of stromatolite layers (chevron-shaped heads) and recovery layers (wavy laminae, no chevron-shaped heads). Capping each stromatolite sequence is an event layer (dark horizontal band). Close-up images of the different types of layers are shown. Eight samples were collected; four from stromatolite and four from event/recovery layers (Note: layer designations are defined in the Results section).

Data (2000) using the DIFFRACplus EVA 13 Evaluation Package.

X-ray fluorescence spectroscopy (XRF)

Concentrations of both major and trace elements for select whole rock samples were determined by the University of Pennsylvania Earth and Environmental Science Department using an XRF instrument. For analysis of major elements, representative samples from each layer were crushed into 0.4 g of rock powder, mixed with 3.6 g of lithium tetraborate (to act as flux), placed in a platinum crucible, and heated until molten. The molten material was then transferred into a platinum crucible and quenched to produce a fused pellet with evenly dispersed sample material for XRF analysis. For analysis of trace elements 7.0 ± 0.0004 g

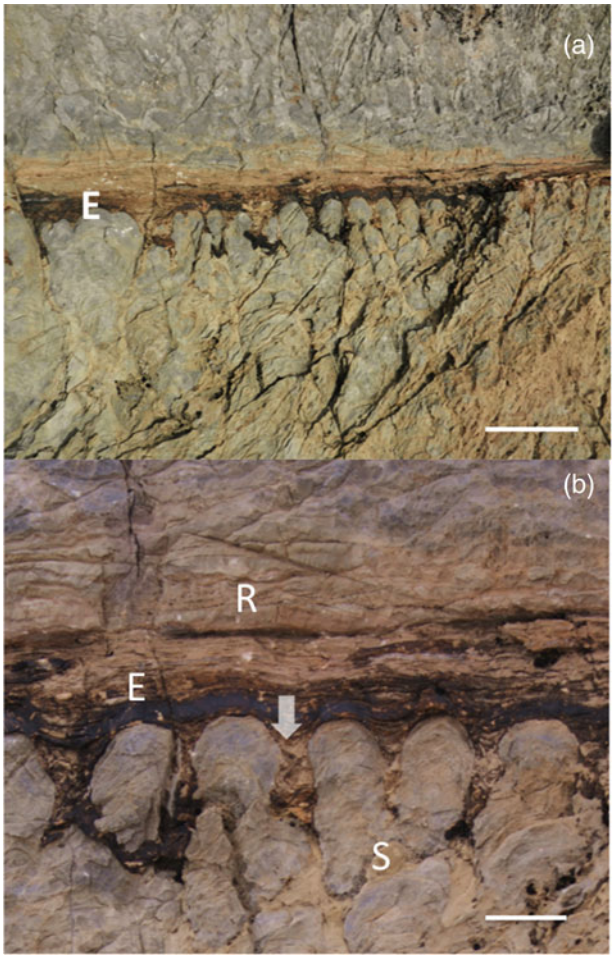

Fig. 3. (a) Field image of a portion of the outcrop, showing an event layer (E), and the top of a stromatolite layer below it (S) and a recovery layer above it (R). (b) Close-up view of the same area as shown in (a). The material forming the event layer can be seen filling the gaps between stromatolite heads (arrow).

of whole rock powder were weighed out and added to 1.40 g of high-purity Copolywax powder, and mixed together for 10 min while pressing the sample.

Environmental scanning electron microscopy-energy dispersive X-ray spectrometry (ESEM-EDS)

The microtextural features of the different layers were compared using an FEI XL30 environmental scanning electron microscope (ESEM), equipped with a high-resolution field emission gun. This instrument was used to analyse both thin sections and pieces of whole rock from the field. A backscattered electron detector allowed discrimination of sample composition based on atomic number through variations in greyscale contrast – the heavier the element, the brighter it appears in images.

Using the ESEM, elemental analysis (EDS) was performed using an EDAX genesis energy-dispersive X-ray spectrometer with an ultrathin window, allowing detection of elements down to and including boron. Detection limits varied from 0.1 wt% at Cu (the element used for calibration) to 0.8 wt% at Si and ~5 wt% at boron as is typical for this type of analysis. The spectrometer was calibrated both for light element detection (C and Al standard, 5 keV) and for standard element detection (Al and Cu, 20 keV).

Results

Field observations

The stromatolites occur as successive layers of laminated, upwardly convex, branching microbial heads separated by zones of unlaminated fine-grained chert-like material (Figs 2 and 3). Stromatolite morphology takes the form of individual chevron-shaped heads. In places, the heads branch to form narrower ones of about half the thickness of unbranched heads. The height of individual heads vary from 14 to 60 cm. Above them are unlaminated layers of fine-grained, orange to dark brown material that appears to 'blanket' the stromatolites, evening out their topography by filling in spaces between the heads (Fig. 3). We called these the 'Event Layers' because they seem to indicate the sudden and rapid burial of the 'Stromatolite Layers' at some point in time. These event layers are harder than the stromatolite layers and therefore more resistant to weathering, thus appearing in positive relief in outcrop. The event layers contain local areas of carbonate that react with dilute HCl, but are mostly composed of a cryptocrystalline, translucent, chert-like material that does not react with HCl, indicating that no detectable carbonate is present. These burials appear to be rapid because the event layers fill in spaces and cover stromatolites without distorting the shape of the stromatolite heads. It is also possible that this sudden burial prevented much water from getting through, explaining the non-silicified nature of the stromatolite layer. Just above these event layers are 'Recovery Layers', horizontal carbonate laminae that gradually become more wavy upwards, and eventually grade into the chevron-shaped heads of the next stromatolite layer. These recovery layers may represent the re-establishment of microbial growth after disruption, first as flat-lying microbial mats and then as larger stromatolites. These successive cycles of event–recovery–stromatolite occur at least five times at our sampling location and appear to be continuous (Fig. 2).

Petrography and mineralogy

The event layers appear to be dominated by a microgranular mosaic of clear, subequant microcline, averaging <10 μm in grain size, cross-cut by secondary veins of hydrothermal carbonate. It should be noted that despite the microcline's low relief and low birefringent nature, identification was complicated by their fine grain size, making reliable optical interference figures difficult to obtain. Further complicating their identification was that they have previously been described in the literature as chert (Roberts 1974), which given their hard, resistant nature in outcrop and their high silica content, as noted by both XRF and ESEM-EDS (see below), is an understandable misidentification. Secondary veins and fractures are filled with a highly birefringent mineral suggestive of calcite

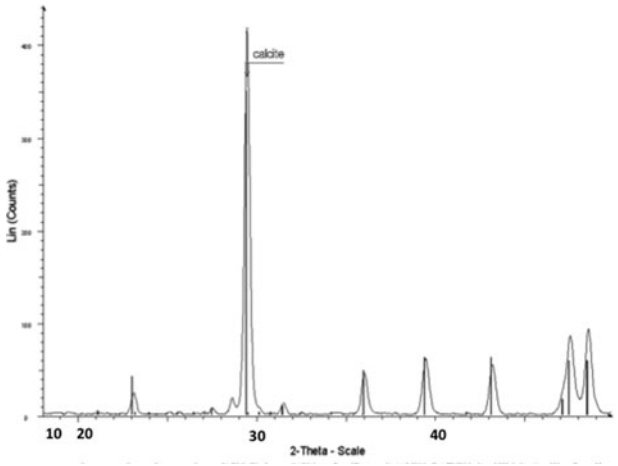

Fig. 4. XRD pattern of the stromatolite layer. All major peaks are attributable to calcite.

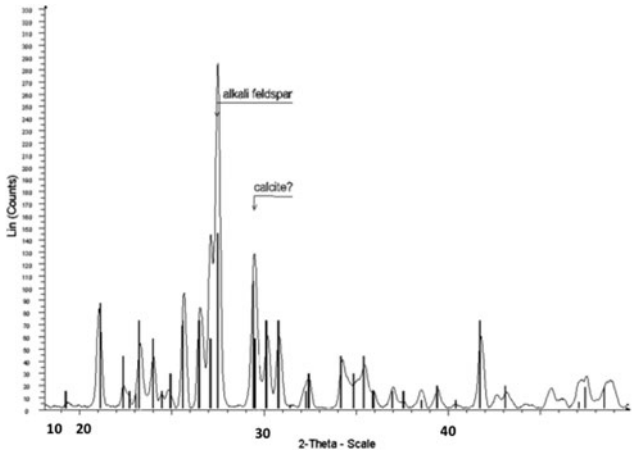

Fig. 5. XRD pattern of the event layer. Almost all the peaks shown are attributable to microcline, a K, Al feldspar.

and/or dolomite. Their hydrothermal nature is consistent with the presence of both Pt and REE elements noted in ESEM (see below) as well as local recystallization along the outer edges of the veins. Both Raman point spectra and bulk mineralogy determined by the XRD confirm the presence of microcline and calcite in these layers Figs 4 and 5.

Geochemistry

The mass fractions, derived from XRF analysis, are given in Table 1 (oxides) and Table 2 (trace elements) for the samples from each of the eight layers. It is clear from these results that the event layers have a distinctly different chemical composition from the stromatolite layers. Si is the major element present in the event layers, while it is very low or absent in the stromatolite layers, which are dominated by Ca. The recovery layers showed a combination of features from both of these two end members as one might expect. This can be seen from the plots in Figs 6 (a) and (b), in which positive correlations between Al, Si and K are shown. Figure 6 (c) shows that Ca and Si are negatively correlated; when Ca content is high, Si content is low. This shows that there is a sharp difference in chemistry and mineralogy between the event layers and the stromatolites. In the stromatolites, another interesting correlation was the direct one between Sc and Ca (Fig. 6(d)).

ESEM-EDS

The ESEM results show that the event layer predominantly consists of fine-grained (<100 μm) minerals composed of K, Al, Si and O with small veins of a mineral comprised the elements Ca, C and O (Fig. 7). These veins do not show discrete grains and have numerous microfissures in them. Small (<5 μm) metal-rich inclusions were sprinkled throughout the event layer. These inclusions were of two types: rare earth element (REE; Ce and La, probably oxides) and Pt (Figs 7 and 8). The stromatolite layer, in contrast, had a distinctly different elemental composition from that of the event layer. Here, distinct mineral grains were visible (Fig. 9), larger than those seen in the event layer and most of these grains were composed of the elements Ca and O by ESEM-EDS (Fig. 10). A number of areas in the sample had an Mg-rich Ca carbonate in the form of blocky grains (Fig. 7). The Mg : Ca ratio in these grains was nearly 1 : 1, suggesting they were dolomite (Fig. 11). Occasional deposits of organic carbon were present in the stromatolite layer, often appearing to penetrate the mass of the stromatolite. These were only found in the stromatolite layer and contained a significant amount of Na, S and Cl. We do not have sufficient data to determine whether this organic matter is penecontemporaneous with the stromatolites, but believe that it is of interest and warrants further investigation. Corkeron *et al.* (2012) noted significant differences between REE compositions in stromatolitic and non-stromatolitic components in some Neoproterozoic stromatolites. It would be useful to compare the REE results obtained here with those from the Bitter Springs Formation stromatolites.

Discussion

The Death Valley succession is composed of an array of diverse stromatolites that have contributed to an understanding of geobiologic history of the Pre-Phanerozoic to the Cambrian (Awramik *et al.* 2000). The branched Crystal Spring Formation stromatolites were formed in a shallow marine setting, and the elliptical shape of the heads indicates growth took place in a current-influenced environment (Roberts 1974). The rock section of interest contains repeated cycles throughout the formation – periods of growth below an event layer representing a change in the environment or change in biology followed by a recovery period with no stromatolites and then, later in the formation, a resurgence of stromatolite growth (see Figs 2 and 3). The older stromatolite sections (the first three sequences) were each 14 cm in height and were morphologically similar, whereas the youngest stromatolite sections (the fourth sequence sampled) looked morphologically different and measured approximately 65 cm in height. Awramik *et al.* (2000) speculated that the lake water was only about 1 m deep at

Table 1. *Inorganic oxide content and elemental concentrations based on XRF data.*

Oxide content (%)	Event 1	Event 4	Event 2	Recovery 4	Recovery 1	Recovery 5	Stromatolite 1	Stromatolite 4
SiO_2	49.03	43.54	65.05	18.51	32.11	33.31	11.22	14.31
TiO_2	0.10	0.22	0.06	0.08	0.08	0.19	0.10	0.06
Al_2O_3	11.29	8.58	16.29	3.23	3.17	8.46	1.12	1.39
Fe_2O3	1.30	1.50	0.49	0.84	0.90	0.76	0.93	0.52
MnO	0.07	0.04	0.06	0.04	0.05	0.06	0.04	0.04
MgO	4.13	9.33	0.36	4.94	3.83	0.55	3.96	0.84
CaO	24.76	29.96	3.02	69.72	56.70	48.78	81.78	81.09
Na_2O	0.10	0.09	0.14	0.05	0.03	0.24	0.03	0.04
K_2O	0.14	0.17	0.23	0.05	0.23	0.24	0.62	0.54
P_2O_5	0.05	0.26	0.09	2.05	0.03	6.35	0.04	0.96

Table 2. *Trace element geochemistry of laminate and non-laminate (Event) layers.*

Oxide content (%)	Event 1	Event 4	Event 2	Recovery 4	Recovery 1	Recovery 5	Stromatolite 1	Stromatolite 4
SiO_2	49.03	43.54	65.05	18.51	32.11	33.31	11.22	14.31
TiO_2	0.10	0.22	0.06	0.08	0.08	0.19	0.10	0.06
Al_2O_3	11.29	8.58	16.29	3.23	3.17	8.46	1.12	1.39
Fe_2O3	1.30	1.50	0.49	0.84	0.90	0.76	0.93	0.52
MnO	0.07	0.04	0.06	0.04	0.05	0.06	0.04	0.04
MgO	4.13	9.33	0.36	4.94	3.83	0.55	3.96	0.84
CaO	24.76	29.96	3.02	69.72	56.70	48.78	81.78	81.09
Na_2O	0.10	0.09	0.14	0.05	0.03	0.24	0.03	0.04
K_2O	0.14	0.17	0.23	0.05	0.23	0.24	0.62	0.54
P_2O_5	0.05	0.26	0.09	2.05	0.03	6.35	0.04	0.96

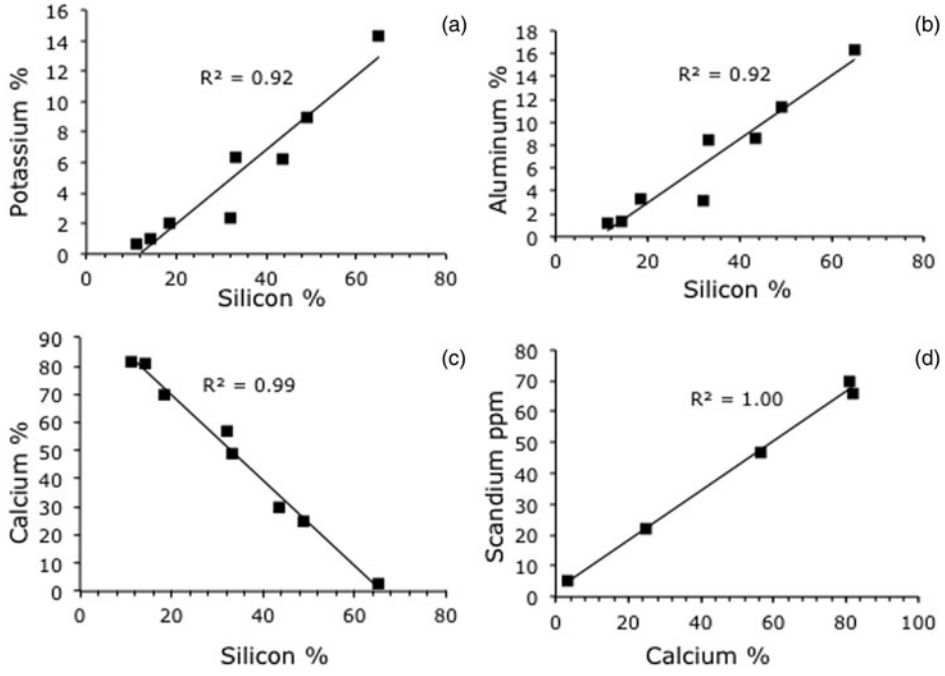

Fig. 6. Correlation between key elements which define the different layers in the formation. There is a positive correlation between Si and K (a) and Si and Al (b), while the correlation between Si and Ca (c) is negative. A positive correlation between Ca and Sc (d) indicates a clear yet undefined relationship between these elements.

the time that the 14 cm high branched stromatolites were deposited, but deeper when the stromatolites grew taller, as they are seen higher in the formation (S. Awramik 2010, personal communication). The original mineralogy of the intervening sediment (event) layers has been obscured by recrystallization of the minerals. Identifying compositional differences between the layers below (with stromatolites) and above (without stromatolites) the intervening layer will provide

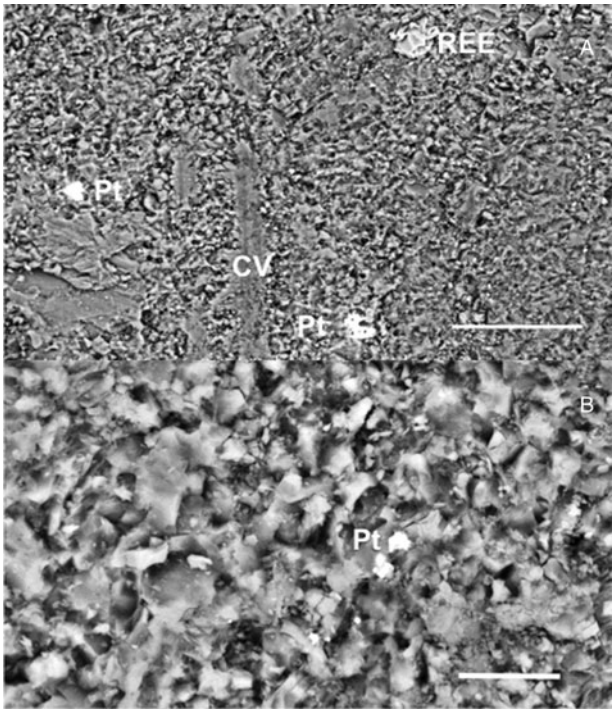

Fig. 7. ESEM images of the event layer at low magnification (a) and higher magnification (b) which show the microstructure and some of the typical inclusions in the event layer: platinum (Pt) and lanthanum–cerium (REE). Several calcite micro veins (cv) are also visible. Bar = 50 μm.

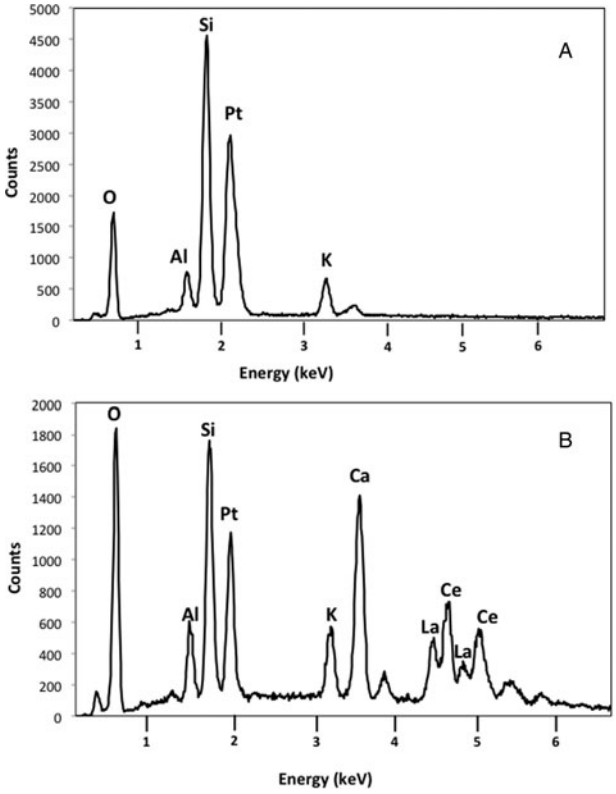

Fig. 8. ESEM-EDS spectra of inclusions in the event layer. (A) Platinum with background of feldspar (K, Al, Si and O). (B) an La–Ce (REE) inclusion in the event layer. Pt is also present.

insight as to what event caused that intervening layer and the subsequent death of the stromatolites below it. The elemental analysis and in particular the anti-correlation between Ca and Si shown in Fig. 6 suggest that the structure of the outcrop section is a record of periods of stromatolite growth (Ca high) that exceeds the input rate of external sandy sediments (Si) and periods of low stromatolite growth compared with sandy sediment flux (Si high, Ca low).

Unusual among stromatolites from the Proterozoic, these structures have not dolomitized or been silicified and are dominated by calcite as their matrix mineral. In many carbonate sediments, calcium is replaced by magnesium, thus forming dolomite $(Ca,Mg)CO_3$. This process can alter or distort the sedimentary and stromatolitic structures and, potentially, their major element and trace metal chemistry. The fact that the minerals and the stromatolites themselves were minimally altered allows us to have some insight into their native chemistry. The Mg concentration seen in these samples varies from 0.3 to 4% and does not correlate with Ca or Si. Thus we conclude that dolomitization is not significant in the Crystal Spring Formation studied, which enables the study of primary sedimentary structures. Analysis of organic material in the same stromatolites by Tanaka *et al.* (2012) shows the presence of relatively young (25 kyr) material presumably deposited when the locale was submerged by a body of water, presumably marine (Roberts 1974). One trace element, Scandium correlated with Ca suggesting some connection – as yet unknown to us – between this element and the biological processes the created the stromatolites.

The presence of a non-laminated intervening layer that neatly fills in the spaces between stromatolite heads and forms a horizontal layer above them implies burial of the stromatolites by some materials. If the material had trickled in slowly, then it is likely that stromatolite organisms would have been able to migrate through it in search of light and kept on growing. In such a case, we would expect several things to have appeared in our data: the appearance of at least partial laminae in the event layer, higher levels of Ca and Sc (markers for the stromatolites) in the event layer, and a mixed texture of the event layer material (both coarse grained and fine-grained) but none of these was seen. We believe the event layers to have formed by a sudden massive input of material.

Without a record of absolute time the data can fit several models of how the environment changed to cause the record seen. On one extreme we can postulate an environment with a constant flux of sandy sediment and variations in the rate of stromatolite growth by calcite precipitation. In this scenario, the stromatolite layers represent periods of high growth and biologically mediated precipitation of calcite. The detrital layers then merely reflect the absence of strong biological growth. The other extreme explanation is that there were significant variations in the flux of material into the system. During periods of low influx the stromatolites were able to grow. Then for some external reason the flux of material was

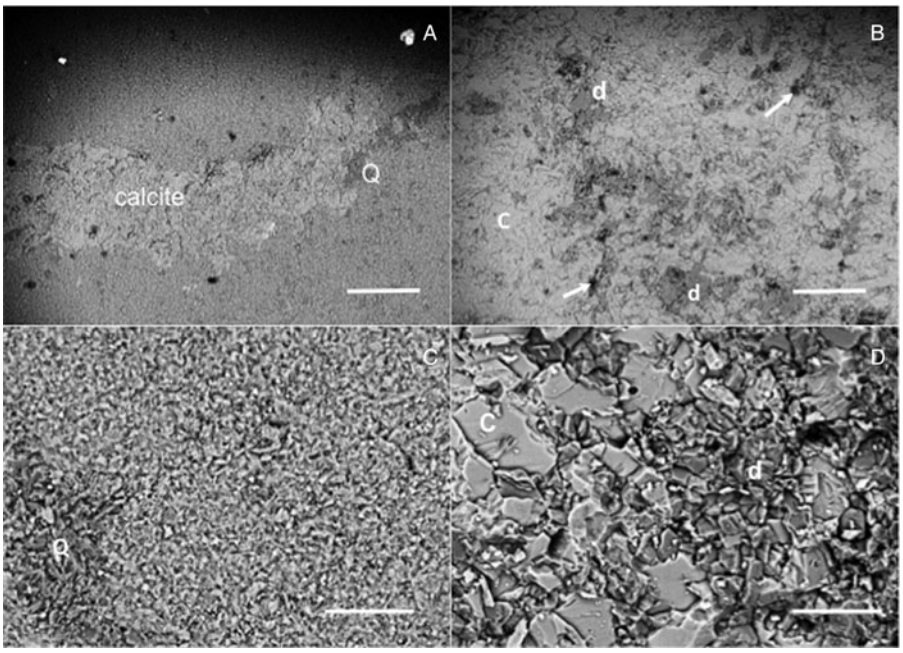

Fig. 9. ESEM images showing the microtextural characteristics of the Event Layer (A and C) as compared with the stromatolite layer (B and D). (A) Event layer showing calcite vein, silicate (quartz or chert, Q) and two heavy element inclusions, one of platinum (Pt) and one of lanthanum–cerium (REE) as given by EDS analysis (see Fig. 5). Bar = 200 μm. (B) Stromatolite sample at the same magnification as the event layer shown in (A). The lighter toned grains are calcite, whereas the darker grey ones (d) are dolomite. Very dark organic matter (e.g. arrows) is also present and tends to occur with the dolomite, with both the dolomite and the organic material being in pores and cracks of the calcite. Bar = 200 μm. (C) Higher magnification (500×) view of the event layer. Note the tightly packed mineral grains with a small size range. The darker diagonal strip in the lower left corner is quartz or chert (Q). Bar = 50 μm. (D) Higher magnification (500×) view of the stromatolite layer. Two compositionally different minerals are shown, calcite (c) and dolomite (d). Note the smaller grain size of the darker dolomite. Bar = 50 μm.

greatly increased and reach a level where it choked off stromatolite growth – possibly by blocking access to sunlight. Either explanation for the layers, controlled by biological growth rates or controlled by the rate of input of detrital material, is consistent with the data. It is a pattern commonly seen in many fossilized stromatolites from all ages and it would be interesting to see if we can see this pattern forming in modern stromatolites.

The concentrations of elements in Table 1 that are associated with Si, particularly K and Al suggest that the main source of detrital material was the weathering of a potassium-feldspar ($KAlSi_3O_8$)-rich rock. The mass fractions of K, Al and Si correspond to a stoichiometry of $K_{0.3}Al_{0.5}Si_3O_8$, in addition a low level of barium feldspars contribute about 0.1% by mass as indicated by the Ba measurements. The usual form of primary $KAlSi_3O_8$ is orthoclase but the weathered product is microcline, a pseudomorph and also a feldspar mineral. Our XRD results showed the predominance of microcline in the event layers, indicating weathered feldspar as detrital material that was carried into the stromatolite zone. It is possible that the microcline is an alteration product of volcanic ash, a possibility that might explain the periodic nature of the material's infall and burial of the stromatolites. If the stromatolites were growing in a shallow body of water and a sudden ash fall occurred the fall of hot ash into the water would have immediately changed the stromatolites' physical and chemical environment. The sudden blanketing of the stromatolites and possibly elevated temperatures may have instantly killed them or at least slowed down their growth. An analogous blanketing by volcanic material has been observed in the 3.4 Gyr old Strelley Pool Formation at the Dawn of Life Trail (Grey *et al.* 2012). As seen in Fig. 3, the Crystal Spring stromatolite heads are well-formed and show no distortion of their shape or their laminae even in the parts right under the event layer. If stromatolite burial had been slow, one would expect to see a region of less distinct, irregularly spaced or laterally discontinuous laminae. Instead, the perfect preservation of shape and lamination implies a rapid burial. The presence of unaltered calcite in the stromatolites may also be attributable to the sudden burial by ash. Owing to its small and uniform grain size plus the presence of both heat and water, the ash would have sealed off the stromatolites, preventing them from being influenced by hydrothermal fluids and allowing them to remain unaltered calcite. However, despite the observation that the event layers had a very small grain size and were permeated by veins of calcite and quartz, we derived no conclusive proof for identification of the burial layer component as volcanic ash-derived material and suggest this as an area for further study.

If an outcrop such as we investigated here (Figs 2 and 3) were viewed by a rover on Mars it would be interesting, but not persuasive evidence of past life. The likely biogenic origin of the stromatolites in the Crystal Spring Formation has been

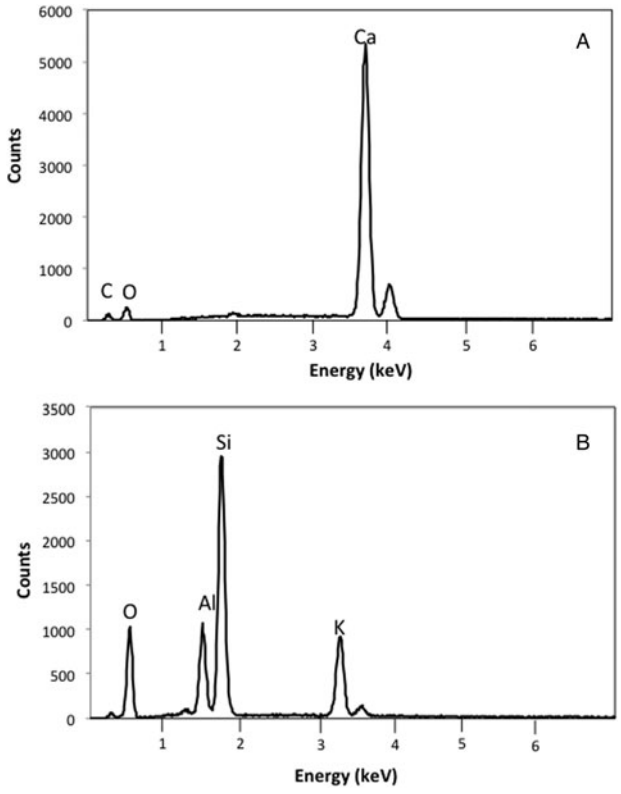

Fig. 10. ESEM-EDS spectra showing the elemental composition of mineral grains from the stromatolite layer (A) and the event layer (B).

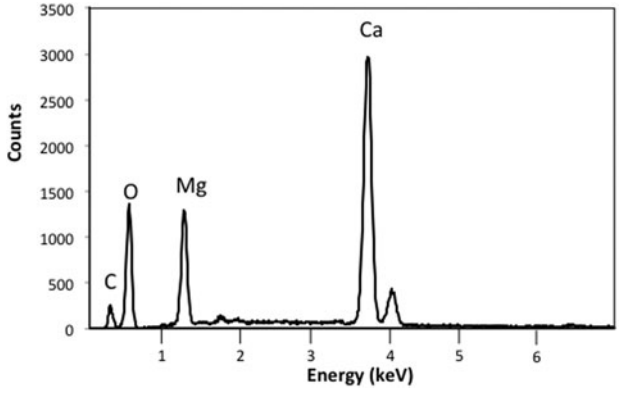

Fig. 11. ESEM-EDS elemental profile of heavier-element mineral grains present both within the event layer and, to a lesser extent, in the stromatolite layer. The elemental signal is consistent with that of dolomite, a Ca, Mg carbonate. Dolomite was present only as occasional grains in the stromatolite matrix.

established by detailed microscopic studies and comparisons to other locations (Howell 1971; Cloud *et al.* 1974; Awramik *et al.* 2000). Three taxa have been named from this formation: Baicalia Krylov 1962; Conophyton Maslov 1937; emend Komar, Raaben and Semikhatov 1965; and Jacutophyton Schapovalova 1965 (see Howell 1971; Roberts 1974; Awramik *et al.* 2005). They were identified only to the Group level (not to the Form level) and the identifications of Conophyton and Jacutophyton are highly questionable because they do not have the conical laminae and axial zones that are mandatory in the diagnosis of these two taxa. The stromatolites appear to conform to the diagnosis of Baicalia, but may be a new Form of this Group. The most recent and accessible reference to the diagnoses of these stromatolite taxa is Raaben *et al.* (2001). Further systematic analysis is required before the stromatolites can be correctly assigned to a Group. However, a Mars rover would be able to conduct a similar organic and mineral analysis to that which we have performed in this paper lending support to a possible biological origin.

Conclusion

In this paper, we have reported on the stratigraphic layering of stromatolites in a vertically extensive outcrop in the Crystal Spring Formation in Southern California. The layering shows four successions of stromatolite formation followed by layers without stromatolite formation. It is worth noting that each of the stromatolitic layers have similar morphologies with regard to size, shape, development of branching, branching patterns, lamina shape and microstructure. In a systematic study, they would all be assigned to a single taxon (probably Baicalia). Elemental analysis of samples from within each of the four stromatolite layers and the four intervening layers shows that the rock is composed of two source materials; calcite stromatolites and K-feldspar sand. In the layers that contain stromatolites the Ca/Si ratio is high. In layers without stomatolites the Ca/Si ratio is low. Other elements follow Si indicating the K-feldspar source for the sand. This characteristic variation between these two sources could be due to variations in biological growth rates in an otherwise uniform environment or variations in sand influx and the resultant impact on biology. The current analysis does not allow us to choose between these two alternatives but it does suggest that further analysis along these lines, perhaps looking more closely at REE given the findings of Corkeron *et al.* (2012), may well provide a suitable approach for differentiating between biogenic and abiogenic structures.

The visible layering we see in the outcrop and the distinctive stromatolite patterns would both be detectable by an imaging system on a Mars rover. The elemental and organic analyses we performed could be conducted on such a rover. Thus we suggest this outcrop as a test location for Mars stromatolite studies.

Acknowledgements

The authors would like to thank Hermann Pfefferkorn for help with thin section analyses, David Vann for help with handheld XRF analyses and thin section preparation, Gomaa Omar for help with XRD analyses and XRD equipment, and University of Pennsylvania Earth and Environmental Science Department, particularly Jane Dmochowski and Robert Giegengack. We would like to

thank Drs Robert Anderson, Rohit Bhartia & Yang Liu of NASA's Jet Propulsion Laboratory for access to, respectively, the X-ray diffractometer, Raman spectrometer and petrographic microscope. Also, the authors would like to thank Ann Copin of JPL Library Services for timely help in gathering reference material. The authors would also like to thank the NASA Spaceward Bound for the field activities. The NASA Astrobiology Institute for funding to support travel and analysis. The NASA Pennsylvania Space Grant Consortium and The Greg and Susan Walker Endowment for funding. We thank the reviewers for specific and useful comments that greatly improved the paper.

References

Allwood, A.C., Walter, M.R., Burch, I.W. & Kamber, B.S. (2007). 3.43 billion-year-old stromatolite reef from the Pilbara Craton of Western Australia: Ecosystem-scale insights to early life on Earth. *Precambrian Research*. **158**, 198–227.

Awramik, S.M., Corsetti, F.A. & Shapiro, R. (2000). Stromatolites and the pre-Phanerozoic to Cambrian history of the area south east of Death Valley. *Bull. San Bernardino County Mus*. **47**(2), 65–74.

Buick, R. (2008). When did oxygenic photosynthesis evolve? *Phil. Trans. R. Soc. B* **363**, 2731–2743.

Cloud, P., Wright, L.A., Williams, E.G., Diehl, P. & Walter, M.R. (1974). Giant Stromatolites and associated vertical tubes from upper Proterozoic noonday dolomite, Death-Valley Region, Eastern California. *Geol. Soc. Am. Bull*. **85**(12), 1869–1882.

Corkeron, M., Webb, G.E., Moulds, J. & Grey, K. (2012). *Discriminating Stromatolite Formation Modes using Rare Earth Element Geochemistry: Trapping and Binding Versus in Situ Precipitation of Stromatolites from the Neoproterozoic Bitter Springs Formation*, vol. **212–213**, pp. 194–206. Northern Territory, Australia: Precambrian Research.

Downs, R.T. (2006). The RRUFF Project: an integrated study of the chemistry, crystallography, Raman and infrared spectroscopy of minerals. *Program and Abstracts of the 19th General Meeting of the Int. Mineralogical Association in Kobe*, Japan.

Grey, K., Clarke, J.D.A. & Hickman, A.H. (2012). The proposed Dawn of Life Geotourism Trail, Marble Bar, Pilbara Craton, Western Australia – geology and evidence for early life: Geological Survey of Western Australia, Record 2012/9, 27p.

Grotzinger, J.P. & Knoll, A.H. (1999) Stromatolites in precambrian carbonates: evolutionary mileposts or environmental dipsticks? *Annu. Rev. Earth Planet. Sci*. **27**, 313–358.

Hickman, A.H. (2011). Pilbara Supergroup of the East Pilbara Terrane, Pilbara Craton: updated lithostratigraphy and comments on the influence of vertical tectonics. Geological Survey of Western Australia. Annual Review 2009–2010, pp. 50–59.

Hofmann, H.J., Grey, K., Hickman, A.H. & Thorpe, R. (1999). Origin of 3.45 Ga coniform stromatolites in Warrawoona Group, Western Australia. *Geol. Soc. Am. Bull*. **111**, 1256–1262.

Howell, D.G. (1971). A stromatolite from the Proterozoic Pahrump group, eastern California. *J. Paleontol*. **45**(1), 48–51.

Lowe, D.R. (1980). Stromatolites 3,400-Myr old from the Archaean of Western Australia. *Nature* **284**, 441–443.

McKay, C.P. (1986). Exobiology and future Mars missions: the search for Mars' earliest biosphere. *Adv. Space Res*. **6**(12), 269–285.

McKay, C.P. & Stoker, C.R. (1989). The early environment and its evolution on mars: implication for life. *Rev. Geohpys*. **27**(2), 189–214.

Raaben, M.E., Sinha, A.K. & Sharma, M. (2001). *Precambrian Stromatolites of India and Russia (a Catalogue of Type-form-genera)*, 125 p. Birbal Sahni Institute of Palaeobotany, Lucknow.

Roberts, M.T. (1974). Stratigraphy and Depositional Environments of the Crystal Spring Formation, Southern Death Valley Region, California. California Division of Mines and Geology Special Report 106.

Tanaka, Z., Perry, M., Cooper, G., Tang, S., McKay, C.P. & Chen, B. (2012). Near-infrared (NIR) Raman spectroscopy of Precambrian carbonate stromatolites with post-depositional organic inclusions. *Appl. Spectrosc*. **66**, 911–916.

Tice, M.M. & Lowe, D.R. (2004). Photosynthetic microbial mats in the 3,416-Myr-old ocean. *Nature* **431**, 549–552.

Wacey, D. (2012). Earliest evidence for life on Earth: an Australian perspective. *Austr. J. Earth Sci*. **59**(2), 153–166.

Walter, M.R., Buick, R. & Dunlop, J.S.R. (1980). Stromatolites, 3,400–3,500 Myr old from the North Pole area, Western Australia. *Nature* **284**, 443–445.